Int. J. Solids Structures Vol. 20, No. 6, pp. 553–570, 1984
Printed in Great Britain.

0020-7683/84 $3.00 + .00

SUPPRESSION OF ANTICLASTIC CURVATURE IN ISOTROPIC AND COMPOSITE PLATES

M. W. HYER and P. C. BHAVANI
Department of Engineering Science and Mechanics, Virginia Polytechnic Institute and State University, Blacksburg, VA 24061, U.S.A.

(*Received* 22 *April* 1983; *in revised form* 8 *August* 1983)

Abstract—This paper discusses the large deflection bending behavior of plates subjected to bending moments along two opposite edges and free on the other two opposite edges. Isotropic and laminated fiber-reinforced composite plates with small initial curvatures are discussed. It is shown that when the applied moments become large, the classical anticlastic saddle shape disappears and the plate flattens laterally to become more cylindrical in nature. This phenomenon is due to nonlinear geometric effects. The theory governing plate behavior and numerical studies illustrating the sensitivity of the plate's flattening response to anisotropy and initial imperfections are presented. Then an experimental apparatus designed to load plates is briefly described. Experimental results are compared with theoretical predictions for a $[(\pm 45)_3]_s$ graphite-epoxy plate, a $[90_2/0_2/\pm 45]_s$ graphite-epoxy plate, and an aluminum plate. Comparison between experiment and theory is shown to be good. Several aspects of the comparison are discussed.

INTRODUCTION

Classical linear plate theory predicts that when a flat square or rectangular isotropic plate is subjected to bending moments along opposite edges, the other two opposite edges being traction-free, two curvatures develop in the plate surface. One curvature, the longitudinal or major curvature, is a direct result of the applied moment and is linearly proportional to it. The other curvature, the lateral or minor curvature, is at right angles to the major curvature and is due to the Poisson effect. The magnitude of the lateral curvature is equal to Poisson's ratio times the magnitude of the longitudinal curvature. This minor curvature is also obviously linearly proportional to the applied moment. The two curvatures, however, are of opposite sign and so the plate deforms into a saddle shape. This saddle-shape phenomenon is referred to as the anticlastic effect. These predictions of the linear theory are confirmed by experimental measurements if the magnitude of the applied moment is small enough that the out-of-plane deflections of the plate are smaller than the plate thickness. If, however, the magnitude of the applied moments is increased so that the plate deflections exceed one plate thickness, behavior that is not quite so well known will be exhibited. Specifically, the saddle-shape anticlastic effect will not occur. Instead of the two curvatures simply increasing in magnitude as the moments are increased, the lateral curvature actually disappears as the longitudinal curvature continues to increase. Due to geometrically nonlinear effects, the plate tends to flatten in the lateral direction. Instead of the plate being saddle shaped, it is more cylindrical in nature, the generators of the cylinder being parallel to the edges experiencing the applied moments. Figure 1 depicts the situation beng described.

Searle[1] was one of the first to present detailed arguments predicting this sort of behavior for isotropic plates. Actually Lamb[2] had discussed this phenomenon several years before Searle. He derived an ordinary differential equation which correctly predicted the phenomenon which was discussed by Searle and which was later measured by other investigators. Ashwell[3], using somewhat heuristic arguments, reiterated Lamb's and Searle's work and derived and solved a governing differential equation similar to Lamb's.

Ashwell and Greenwood[4] conducted an experiment to verify some of Ashwell's theoretical predictions. They used a mild steel plate and, unfortunately, the plate was not initially flat. The plate had an initial curvature which provided an additional geometric stiffness to the plate. This significantly changed the response of their plate. Ashwell[5], using von Karman plate theory as a starting point, developed a theory which accounted for initial curvatures. Once the initial curvatures had been accounted for, the suppression of the lateral

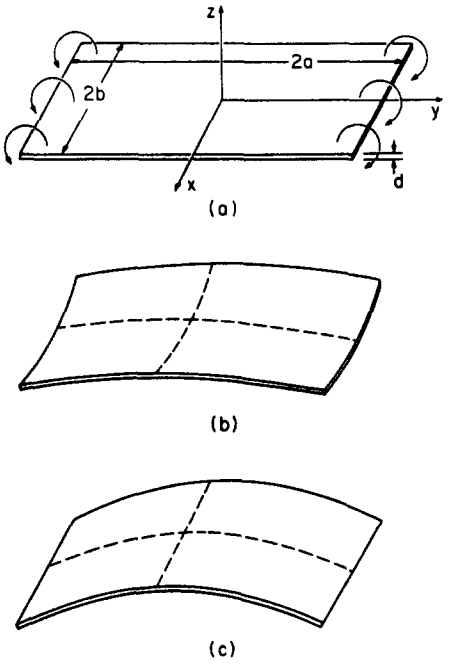

Fig. 1. Problem description; (a) plate loading and geometry, (b) saddle shape of linear theory, (c) flattening in lateral direction due to geometric nonlinearities.

anticlastic curvature was accurately predicted. The experimental data presented was quite limited, being limited to one plate at one moment level.

Gerard[6] amplified Ashwell's early work and Fung and Wittrick applied Ashwell's ideas to plates of variable thickness[7] and plates with trapezoidal and rhombic planforms[8]. Cantilever plates and plates loaded by point loads at the corners were also studied by Fung and Wittrick[8]. Pomeroy[9] presented expressions for the effect of the lateral flattening on the longitudinal moment-curvature relation. All of these studies were theoretical. Bellow *et al.*[10] conducted experiments to measure the flattening tendency. They used strain gages and integrated the strains numerically to obtain out-of-plane deflections. This idea produced results that agreed quite well with Ashwell's predictions. Bellow *et al.* found that initial imperfections in the plate did not influence their results.

Pao[11] has been the only investigator to begin to address these issues for composite plates. Pao studied two layer cross-ply and angle-ply fiber-reinforced plates which were assumed to be initially flat. Pao followed the ideas put forth by Ashwell[5] but, due to the anisotropy of the plate, the situation was somewhat more complex. More importantly, because Pao considered the case of two plies, there was an inherent material coupling between the inplane and the out-of-plane deflections. Ultimately Pao derived an ordinary differential equation similar to Ashwell's. Pao showed that for two-ply plates the lateral anticlastic curvature was suppressed when the plate deflections became large. In addition, the fiber angles in the two plies could be used to control the degree and character of the suppression. The work of Pao, though lacking experimental confirmation, was important. Controlling the degree of suppression of the lateral curvature might be advantageous in certain applications. Pao demonstrated that the suppression could be controlled by fiber orientation. This is an effect impossible to achieve in isotropic materials. Furthermore, Pao considered unsymmetric laminates, a stacking arrangement not in common usage. With unsymmetric laminates, he may have predicted effects that cannot be achieved even with symmetric laminates. His work is important for another reason. Pao was one of the earliest investigators to consider nonlinear geometric effects in composite plates. Composite plates are more likely to experience nonlinear geometric effects than plates fabricated from metals. There are two reasons for this. First, composite materials remain linear elastic to much higher strain levels than metals. In designing to maximum strain levels, larger strains

and thus larger deflections are permitted with composite structures than with metal structures. Second, because of the high strength properties of composite materials, minimum gage construction is possible. Thus composite structures may well experience fairly large deflections under a given load. By extending the previous theory of isotropic plates to composites, Pao rightfully considered a situation where large deflections could be a common occurrence. There were two limitations to Pao's work. First, Pao assumed that the plates under investigation were initially flat. It is virtually impossible to fabricate a flat composite plate. Slight differences in ply thicknesses, lack of perfectly straight fibers, inadvertent misalignment of a particular lamina, spatial variations in volume fraction of fiber and matrix, lack of uniform curing, and a host of other problems can and do prevent fabrication of perfectly flat laminated plates. In his study of isotropic plates Ashwell showed that a slight initial lateral curvature can make a large difference in the response of an isotropic plate to a given applied moment. Realistically, then, for composite plates initial curvatures need to be considered. The second limitation of Pao's work is that he conducted no experiments to verify his findings. The experiments would not have been that easy since flat unsymmetrically laminated plates are difficult to fabricate. This difficulty is aside from the difficulties, just mentioned, that are related to variations in ply thickness, lack of straight fibers, etc. It has been shown recently by Hyer[12–14] that unsymmetrically laminated plates which are flat at their elevated cure temperature become cylindrical when they are cooled to room temperature. Love and Ashton[15], however, fabricated flat unsymmetrically laminated plates by bonding together two symmetrically laminated plates with a room-temperature cure adhesive. Pao did not address the issue of actually producing the plates he was modeling. His results are thus only predictions.

It was the main purpose of the work reported on here to study experimentally the suppression of anticlastic effects in composite plates. Because no experimental work had been done at all with composite plates, the experimentally easier case of symmetrically laminated plates was studied. In addition, since initial curvatures are so common in composite plates, Pao's theory was extended to include initial lateral and longitudinal curvature. This paper describes the extended theory, the apparatus used to load the plates and measure their deflection characteristics, and selected numerical results. The numerical results illustrate the nonlinear plate response and indicate the sensitivity of the plate's response to the initial imperfections and the fiber orientations. Finally, for three different plates, theoretical predictions are then compared with experimental results. The first plate discussed is a $[(\pm 45)_3]$, graphite-epoxy plate. The second plate discussed is a $[(90_2/0_2/\pm 45)]$, plate, also of graphite-epoxy. The third plate is an isotropic aluminum plate. This plate, which was chosen to be very close in thickness to the composite plates, was studied to put the results for the composite plates into context. Since the theoretical development parallels the earlier works of Ashwell[5] and Pao[11], only the highlights of the development are presented.

GOVERNING EQUATIONS

A standard cartesian coordinate system, as shown in Fig. 1, is used in deriving the governing equations. The x-y plane coincides with the geometric midplane of an initially flat undeformed plate. The undeformed plate has dimensions $2a$ in the longitudinal direction, $2b$ in the lateral direction, and has thickness d. The independent spatial variable in the longitudinal direction is y while x is the independent spatial variable in the lateral direction. The spatial variable z is perpendicular to the x-y plane. (In the stacking sequence notation used here, the fiber angle is referred to the $+x$ axis and the left most entry refers to the outer layer of the plate.) The displacements in the x, y, z directions will be denoted by u, v, and w respectively. In laminated plate theory the kinematics of deformation are defined in terms of the kinematics of the plate's geometric midsurface. In the nomenclature here, the x-direction displacement of the midplane is $u^0(x, y)$, the y-direction displacement is $v^0(x, y)$, and the z-direction displacement is $w(x, y)$. These variables are considered the total response of the plate. Due to initial imperfections in the plate, an initial out-of-plane displacement of the midplane exists and is denoted as $w_0(x, y)$. Initial inplane displacements of the midplane are assumed to be zero. In deriving the governing equations, all assumptions

pertinent to classical laminated plate theory, as presented in standard reference texts[16], are in effect except one. The one exception is the strain-displacement relations. Instead of using the linear strain-displacement relations, the geometric effects associated with large deformations and the initial imperfections require the pertinent strain-displacement relations to take the form

$$\epsilon_x = \epsilon_x^0 + z\kappa_x, \epsilon_y = \epsilon_y^0 + z\kappa_y, \gamma_{xy} = \gamma_{xy}^0 + z\kappa_{xy}, \tag{1a–c}$$

where

$$\epsilon_x^0 = u_{,x}^0 + \frac{1}{2}\{w_{,x}^2 - w_{0,x}^2\}, \epsilon_y^0 = v_{,y}^0 + \frac{1}{2}\{w_{,y}^2 - w_{0,y}^2\}, \tag{2a,b}$$

$$\gamma_{xy}^0 = u_{,y}^0 + v_{,x}^0 + \{w_{,x}w_{,y} - w_{0,x}w_{0,y}\}, \tag{2c}$$

$$\kappa_x = -(w_{,xx} - w_{0,xx}), \kappa_y = -(w_{,yy} - w_{0,yy}) \text{ and } \kappa_{xy} = -2(w_{,xy} - w_{0,xy}). \tag{3a–c}$$

Enforcing equilibrium of a differential plate element and properly accounting for geometrically nonlinear effects results in the following well-known equations:

$$N_{x,x} + N_{xy,y} = 0, N_{xy,x} + N_{y,y} = 0 \tag{4a,b}$$

$$N_x w_{,xx} + 2N_{xy}w_{,xy} + N_y w_{,yy} + Q_{x,x} + Q_{y,y} = 0 \tag{4c}$$

$$M_{x,x} + M_{xy,y} = Q_x, M_{xy,x} + M_{y,y} = Q_y. \tag{4d,e}$$

In the above $N_x, \ldots, M_{xy}$ are the force and moment resultants and have the usual definition, e.g.

$$N_x = \int_{-d/2}^{d/2} \sigma_x \, dz, \ldots, M_{xy} = \int_{-d/2}^{d/2} \tau_{xy} z \, dz. \tag{5}$$

The quantities Q_x and Q_y are the through-the-thickness shear stress resultants and can be considered to be defined by eqns 4(d,e), respectively. Integrating Hooke's Law through the thickness of the laminate leads to the relation between the force and moment resultants and the midplane strains and curvatures. This relation involves the A, B and D matrices of laminated plate theory[16] and takes the form

$$\begin{Bmatrix} N \\ M \end{Bmatrix} = \begin{bmatrix} A & B \\ B & D \end{bmatrix} \begin{Bmatrix} \epsilon^0 \\ \kappa \end{Bmatrix}. \tag{6}$$

The pertinent boundary conditions in the problem are:

$$\text{at } x = \pm b, N_x = N_{xy} = Q_x - M_{xy,y} = M_x = 0 \tag{7a–d}$$

$$\text{at } y = \pm a, N_y = N_{xy} = Q_y - M_{xy,x} = 0, M_y = \text{applied}. \tag{7e–h}$$

Here interest is more in the out-of-plane displacement, $w(x, y)$, than in the two inplane displacements u^0 and v^0. As is often done, u^0 and v^0 are eliminated from the problem by introducing a stress function of the form

$$\phi_{,yy} = N_x, \phi_{,xx} = N_y, \phi_{,xy} = -N_{xy} \tag{8a–c}$$

and enforcing compatibility of the midsurface strains. That compatibility equation is

$$\epsilon_{x,yy}^0 + \epsilon_{y,xx}^0 - \gamma_{xy,xy}^0 = (w_{,xy}^2 - w_{0,xy}^2) - (w_{,xx}w_{,yy} - w_{0,xx}w_{0,yy}). \tag{9}$$

Using the partially inverted form of eqn (6), namely,

$$\begin{Bmatrix} \epsilon^0 \\ M \end{Bmatrix} = \begin{bmatrix} A^{-1} & -A^{-1}B \\ BA^{-1} & D-BA^{-1}B \end{bmatrix} \begin{Bmatrix} N \\ \kappa \end{Bmatrix} = \begin{bmatrix} A^* & B^* \\ -(B^*)^T & D^* \end{bmatrix} \begin{Bmatrix} N \\ \kappa \end{Bmatrix}, \tag{10}$$

eqn (9) and the last three of eqn (4) can be used to find two equations for $\phi(x, y)$ and $w(x, y)$. These equations are:

$$\begin{aligned} &A^*_{22}\phi_{,xxxx} - 2A^*_{26}\phi_{,xxxy} - 2A^*_{16}\phi_{,xyyy} + A^*_{11}\phi_{,yyyy} + (2A^*_{12} + A^*_{66})\phi_{,xyxy} \\ &\quad = B^*_{12}(w_{,xxxx} - w_{0,xxxx}) + (2B^*_{26} - B^*_{16})(w_{,xxxy} - w_{0,xxxy}) \\ &\qquad + (B^*_{11} + B^*_{22} - 2B^*_{66})(w_{,xxyy} - w_{0,xxyy}) + (2B^*_{16} - B^*_{26})(w_{,xyyy} - w_{0,xyyy}) \\ &\qquad + B^*_{12}(w_{,yyyy} - w_{0,yyyy}) - (w_{,xx}w_{,yy} - w_{0,xx}w_{0,yy}) + ((w_{,xy})^2 - (w_{0,xy})^2); \end{aligned} \tag{11}$$

$$\begin{aligned} &B^*_{21}\phi_{,xxxx} + (2B^*_{26} - B^*_{16})\phi_{,xxxy} + (B^*_{11} + B^*_{22} - 2B^*_{66})\phi_{,xxyy} + (2B^*_{16} - B^*_{26})\phi_{,xyyy} \\ &\quad + B^*_{12}\phi_{,yyyy} - \phi_{,xx}w_{,yy} + 2\phi_{,xy}w_{,xy} - \phi_{,yy}w_{,xx} + D^*_{11}(w_{,xxxx} - w_{0,xxxx}) + 4D^*_{16}(w_{,xxxy} - w_{0,xxxy}) \\ &\quad + 2(D^*_{12} + 2D^*_{66})(w_{,xxyy} - w_{0,xxyy}) + 4D^*_{26}(w_{,xyyy} - w_{0,xyyy}) + D^*_{22}(w_{,yyyy} - w_{0,yyyy}) = 0. \end{aligned} \tag{12}$$

Equations (11) and (12) are the two equations of interest. Obviously their complexity presents difficulties in seeking closed-form solutions. However, as is often the case, certain physically-motivated simplifying assumptions can be made in the context of the particular problem to which they are being applied. These assumptions then make it possible to obtain approximate solutions to the equations. These approximations and the resulting solutions are discussed next.

SOLUTIONS TO GOVERNING EQUATIONS

As stated earlier, concern here was with symmetrically laminated plates. Therefore

$$B^*_{ij} = 0 \quad \text{and} \quad D^*_{ij} = D_{ij} \quad i, j = 1, 2, 6. \tag{13a, b}$$

Furthermore the laminates studied experimentally were balanced and, of course, aluminum is isotropic, so

$$A_{16} = A_{26} = 0. \tag{13c}$$

These facts significantly simplify the two governing equations, eqns (11) and (12). If attention is focused on the central portion of the plate, away from the applied moments, the functional form of $w(x, y)$ can be approximated and further simplifications are possible. The simplifications are as follows: Away from the applied moments, the variation of the out-of-plane deflection with the lateral coordinate, x, is essentially independent of the longitudinal coordinate, y. Furthermore, in the central portion of the plate the applied moments can be assumed to cause a constant curvature in the longitudinal direction. Combining these ideas, $w(x, y)$ is taken to be in the form

$$w(x, y) = w_1(x) + \frac{y^2}{2R_y}. \tag{14}$$

The function $w_1(x)$ represents the functional dependence of the out-of-plane deflections on the x coordinate in the central portion of the plate. The radius of curvature of the central portion of the plate in the longitudinal direction is R_y. It will be assumed R_y is a known quantity. In the experiments, with moments applied to the plate, R_y will be measured. Then w_1 will be measured as a function of x. For the linear problem

$$w_1(x) = -\frac{\nu x^2}{2R_y}. \tag{15}$$

Using the simplifications of eqns (13) and (14), the two governing equations, eqns (11) and (12), become

$$A_{22}^{*}\phi_{,xxxx} + A_{11}^{*}\phi_{,yyyy} + (2A_{12}^{*} + A_{66}^{*})\phi_{,xyxy} = -\left(\frac{1}{R_y}\frac{d^2w_1}{dx^2} - w_{0,xx}w_{0,yy}\right) - (w_{0,xy})^2, \quad (16)$$

and

$$-\phi_{,xx}\frac{1}{R_y} - \phi_{,yy}\frac{d^2w_1}{dx^2} + D_{11}\left(\frac{d^2w_1}{dx^4} - w_{0,xxxx}\right) - 4D_{16}w_{0,xxxy} - 2(D_{12} + 2D_{66})(w_{0,xxyy}) - 4D_{26}(w_{0,xyyy}) - D_{22}(w_{0,yyyy}) = 0. \quad (17)$$

Several other physical factors can be used to further simplify the above equations. The first concerns the initial imperfection, $w_0(x, y)$, the second concerns the y dependence of certain other important variables in the problem, and the third concerns the relative magnitude of the effects of the inplane stress resultants.

For most laminated plates made to be flat, the deviation from flattness is generally a mild half-wave type bowing of from one-half to one plate thickness in magnitude. Generally this bowing results in a small longitudinal curvature, a small lateral curvature, and a small twist curvature. Here, the twist curvature was ignored and the intial imperfections in the plates were taken to be of the form

$$w_0(x, y) = \frac{x^2}{2R_{x_0}} + \frac{y^2}{2R_{y_0}}. \quad (18)$$

The quantities R_{x_0} and R_{y_0} represent the initial lateral and longitudinal radii of curvature due to imperfections. They are assumed to be constant over the area of the plate. Observation of actual plates fabricated to be flat indicates that this a reasonable first approximation. Questions could be raised, however, about ignoring the twisting curvature. As will be seen, these assumptions worked quite well, R_{x_0} and R_{y_0} being measured experimentally. Concerning the y dependence of certain variables, it is quite accurate to assume that near the center of the deformed plate, the stress and moment resultants are independent of the longitudinal coordinate, y. Specifically, because of this independence,

$$N_{x,y} = \phi_{,yyy} = 0 (\text{implies } \phi_{,yyyy} = 0),\ N_{xy,y} = \phi_{,xyy} = 0 (\text{implies } \phi_{,xyxy} = 0), \quad (19a,b)$$

$$\phi_{,xxxx} = N_{y,xx} = aa\frac{d^2N_y}{dx^2}. \quad (19c)$$

Finally, at the $x = \pm b$ edges of the plate, $N_x = 0$. Because of this, throughout the central region $N_x (= \phi_{,yy})$ can be expected to be small compared to $N_y (= \phi_{,xx})$, particularly if the plate is long. In addition, if the plate does indeed flatten in the x direction as the applied moments increase, then the curvature in the x direction, (d^2w_1/dx^2), will be small compared to the curvature in the y direction, $(1/R_y)$. As a result of these magnitude arguments

$$\phi_{,yy}\left(\frac{d^2w_1}{dx^2}\right) < \phi_{,xx}\left(\frac{1}{R_y}\right) \quad (20)$$

and the product on the left is assumed to be zero relative to the product on the right. Using eqns (18), (19), and (20) in eqns (16) and (17), and using the definition of N_y, results in two equations:

$$A_{22}^{*}\frac{d^2N_y}{dx^2} + \frac{1}{R_y}\frac{d^2w_1}{dx^2} = \frac{1}{R_{x_0}}\frac{1}{R_{y_0}}, D_{11}\frac{d^4w_1}{dx^4} - \frac{N_y}{R_y} = 0. \quad (21a,b)$$

Integrating eqn (21a) twice results in

$$N_y = -\left(\frac{1}{A_{22}^{*}R_y}\right)w_1 + \left(\frac{1}{A_{22}^{*}R_{x_0}R_{y_0}}\right)\frac{x^2}{2} + C_1x + C_2. \quad (22)$$

With the symmetries of the applied load, the plate geometry, the assumed initial imperfections, and the plate material properties, N_y must be an even function of x. Thus

$$C_1 = 0. \tag{23}$$

Substituting eqn (22) into (21b) results in

$$\frac{d^4 w_1}{dx^4} + \left(\frac{1}{A_{22}^* D_{11} R_y^2}\right) w_1 = \left(\frac{1}{A_{22}^* D_{11} R_y R_{x_0} R_{y_0}}\right)\frac{x^2}{2} + \frac{C_2}{D_{11} R_y}. \tag{24}$$

This equation governs the variation of the out-of-plane displacement as a function of the lateral coordinate, x. When $R_{x_0} \to \infty$ and $R_{y_0} \to \infty$, the plate is initially flat and the first term on the right hand side disappears. This resulting equation is, of course, similar to the one obtained by Pao. Again, due to symmetries only solutions to $w_1(x)$ symmetric in x are being sought. The pertinent solution to eqn (24), in terms of nondimensional variables, is

$$W(X) = A \cosh(\alpha X)\cos(\alpha X) + B \sinh(\alpha X)\sin(\alpha X) + \frac{b^2 R_y}{2dR_{x_0}R_{y_0}} X + \frac{C_2 A_{22}^* R_y}{d}, \tag{25}$$

where

$$W = w_1/d, \quad X = x/b, \quad \alpha = \sqrt[4]{\frac{b^4}{4A_{22}^* D_{11} R_y^2}}. \tag{26a-c}$$

The constants A, B, and C_2 must be determined by application of the appropriate boundary conditions from among eqn (7). This is done next.

Since attention has been focused on the portion of the plate away from the applied moments, conditions at $y = \pm a$ cannot be strictly enforced. However, the final solution of $w_1(x)$ cannot grossly violate any of the conditions there and so these conditions must be kept in mind. At $x = \pm b$, eqns (7a, b) are not too useful since they involve u_0 and v^0, quantities which have been eliminated. However, as they involve only w, eqns 7(c, d) do provide useful information. Since it is being assumed the force and moment resultants do not vary with y, eqns (7c) simplifies and the two boundary conditions with which to determine A and B, are

$$Q_x = 0 \quad \text{and} \quad M_x = 0 \quad \text{at} \quad x = \pm b. \tag{27a,b}$$

By eqn (4d), eqn (27a) implies

$$M_{x,x} = 0. \tag{27c}$$

Using eqns (25) and (26) in eqn (14), and using eqn (18), the fourth of eqn (6) can be used to find expressions for M_x and hence Q_x. Enforcing eqns (27b,c) with these expressions leads to

$$A = -H\left(\frac{\sinh\alpha\cos\alpha - \cosh\alpha\sin\alpha}{\sinh 2\alpha + \sin 2\alpha}\right), \quad B = -H\left(\frac{\sinh\alpha\cos\alpha + \cosh\alpha\sin\alpha}{\sinh 2\alpha + \sin 2\alpha}\right), \tag{28a,b}$$

with

$$H = \frac{1}{d}\left\{\frac{D_{12}}{D_{11}}\left(\frac{1}{R_y} - \frac{1}{R_{y_0}}\right) + \frac{1}{R_{x_0}}\left(\frac{R_y}{R_{y_0}} - 1\right)\right\}. \tag{28c}$$

The constant C_2 can be determined by examining eqns (22) and (25). Substituting for $w_1(x)$

from eqns (25), (26), and (28) into eqn (22), it is seen that C_2 is not actually involved in the determination of N_y. In addition, from eqn (25) it is clear that C_2 represents a simple rigid body translation of the plate and is thus immaterial. Therefore C_2 is arbitrary and so it is chosen to be zero, i.e.

$$C_2 = 0. \tag{29}$$

This completes the solution for $w_1(x)$. As mentioned previously, it is assumed the longitudinal curvature R_y is a known independent parameter. In reality it is caused by the applied moments. It is useful for experimental comparison to have an expression for the relation between R_y in the central portion of the plate and the applied moment. Because the plate deflections are finite, the moment in the central portion of the plate is given by

$$M_y(\text{total}) = \int_{-b}^{b} N_y w_1 \, dx + \int_{-b}^{b} M_y \, dx. \tag{30}$$

Substituting for N_y and M_y from eqn (6) in terms of w_1, w_0, etc. and integrating, a lengthy expression for M_y(total) results. The expression is:

$$\begin{aligned} M_y(\text{total}) = \frac{-d^2}{R_y A_{22}^{-1}} \Bigg\{ \frac{b\mu}{8\alpha} + \frac{b^3 R_y}{dR_{x_0} R_{y_0}} \Bigg(\frac{1}{5} + \frac{1}{\alpha^2} \Bigg[& (A-B)\alpha \sinh\alpha \cos\alpha \\ & + (A+B)\alpha \cosh\alpha \sin a - \frac{\lambda}{\alpha} - 2(A \sinh\alpha \sin\alpha - B \cosh\alpha \cos\alpha) \Bigg] \Bigg) \Bigg\} \\ & - 2D_{12} \left(\frac{d\alpha\lambda}{b} \right) - \frac{2D_{12} b R_y}{R_{x_0} R_{y_0}} + 2b \left\{ \frac{D_{12}}{R_{x0}} - \frac{D_{22}}{R_y} + \frac{D_{22}}{R_{y0}} \right\}. \end{aligned} \tag{31}$$

where

$$\begin{aligned} \mu = & \{2(A^2 - B^2)[\sinh 2\alpha + \sin 2\alpha] + 4\alpha(A^2 - B^2) \\ & + (A^2 - B^2 + 2AB)\cosh 2\alpha \sin 2\alpha + (A^2 + B^2 - 2AB)\sinh 2\alpha \cos 2\alpha\} \\ \lambda = & \{(A+B)\sinh\alpha \cos\alpha - (A-B)\cosh\alpha \sin\alpha\}. \end{aligned} \tag{32}$$

Using eqn (31) it is possible to determine what value of applied moment is necessary to produce a given longitudinal radius of curvature R_y.

NUMERICAL RESULTS

Before reporting on the experimental aspects of the study, it is instructive to examine several cases that reveal the effects of the non-linearity and the effects of the imperfections on a plate's out-of-plane deflections. Figure 2 shows the effects of the nonlinearities on the cross-sectional displacements of an initially flat $[(\pm 45)_3]_s$ plate. The figure shows the out-of-plane deflection, $w_1(x)$, as a function of x at the $y = 0$ location. The quantities have been normalized as in eqn (26) and the response is shown for several longitudinal radii of curvature. Recall that the longitudinal radius of curvature is being considered as the independent variable. Note that the cross-sectional shapes shown in Fig. 2 are oriented as would be observed for the situation depicted in Fig. 1.

For the case $R_y = -1000$ in., linear theory predicts a lateral peak-to-peak non-dimensional deflection of 0.14. This is essentially the case in Fig. 2. By the linear theory, changing R_y to -300 and -100 should change the peak-to-peak deflections proportionately. Specifically the lateral peak-to-peak deflections should increase by 3.33 and 10, respectively, to 0.46 and 1.4. Due to nonlinear effects, this is not the case. The plate is actually much flatter in the lateral direction than linear theory predicts. In fact, for the case $R_y = -40$, the lateral peak-to-peak deflections are an order of magnitude smaller than the predictions of the linear theory. Also, for the nonlinear case of $R_y = -40$, the lateral peak-to-peak deflections are at least an order of magnitude smaller than the longitudinal

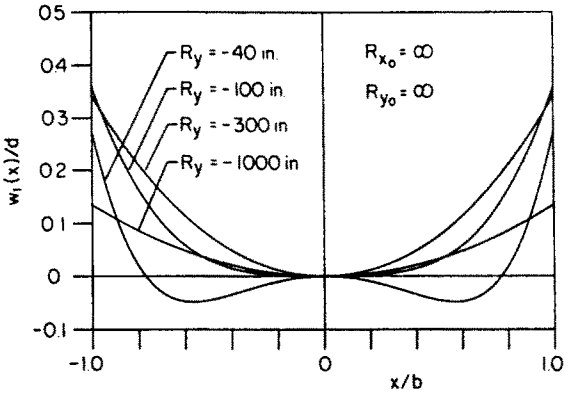

Fig. 2. Effects of nonlinearities on the deflections of an initially flat $[(\pm 45)_3]_s$ plate.

peak-to-peak deflections measured from $y/b = 0$ to $y/b = 1.0$. Figure 2 is representative of the theoretical predictions for the $[(90_2/0_2/\pm 45_2)]_s$ and aluminum plates. Similar studies were conducted for laminates in the family $[(\pm\theta)_3]_s$, θ varying in 15° increments from 0° to 90°. For a plate with all the fibers in the lateral direction, a 0_{12} laminate, nonlinear effects were very weak. For a plate with all the fibers in the longitudinal direction, a 90_{12} laminate, nonlinear effects were quite strong. For the other laminates in the family, the strength of nonlinear effects varied with θ.

Figure 3 shows the effects of an initial lateral curvature on the character of the cross-sectional displacements for a $[(90_2/0_2/\pm 45)]_s$ plate. Figure 4 shows the same information for a $[(\pm 45)_3]_s$ plate. In both figures the plate is assumed to be initially flat in the longitudinal direction. Moments are applied so that $R_y = -40$ in. and so the plate response is in the nonlinear range. For each laminate, the effects of three initial lateral curvatures, +300, 0, and −300 in., are shown. A value of 300 in. for the initial lateral radius was used because this was representative of the values found in actual plates. The sign of the curvature was studied because a plate could be warped either way relative to the applied moments. As can be seen, the $(90_2/0_2/\pm 45)_s$ plate is more sensitive to an initial lateral curvature than is the $[(\pm 45)_3]_s$ plate. For the $[(90_2/0_2/\pm 45)]_s$ plate, the sign of the deflection at the free edges (at $x/b = \pm 1$) depends on the initial radius of curvature. For the $[(\pm 45)_3]_s$ plate, only the magnitude of the deflection at the free edge was sensitive to the sign of the initial imperfection. The $[(\pm\theta)_3]_s$ family of plates was studied for imperfection sensitivity. The cases $\theta = 0°$, 15°, and 30° were quite sensitive to the sign of the initial lateral imperfection. The other laminates were insensitive. The aluminum plate was slightly more sensitive to the effects of the initial lateral imperfection than the $[(\pm 45)_3]_s$ plate was. These sorts of numerical studies were conducted not only to gain insight into the problem but also to guide the choice of stacking sequences to examine experimentally.

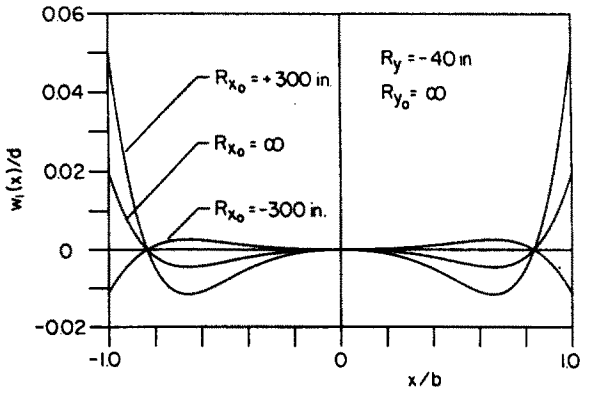

Fig. 3. Effects of initial lateral curvature on the deflections of a $[90_2/0_2/\pm 45]_s$ plate which has no initial longitudinal curvature.

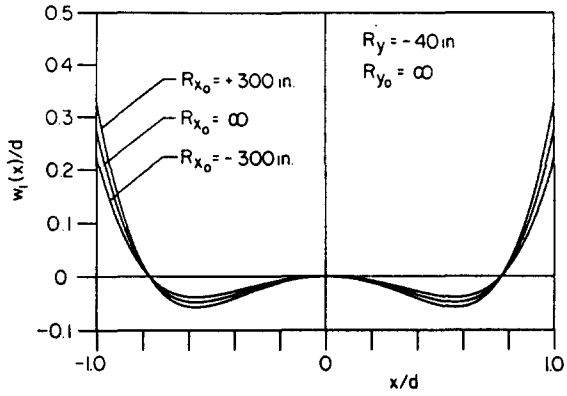

Fig. 4. Effects of initial lateral curvature on the deflections of a $[(\pm 45)_3]_t$ plate which has no initial longitudinal curvature.

Figure 5 and 6 show the effects of initial longitudinal curvature on the character of the out-of-plane deflections. An initial lateral radius of curvature of 300 in. was chosen for each case. Initial longitudinal radii of curvature +300 in., ∞, and −300 in. were studied. Again it was assumed in each case that the applied moments caused a radius of curvature of $R_y = -40$ in. in the longitudinal direction. As can be seen, in the presence of an initial lateral curvature, the $[(90_2/0_2/\pm 45)_3]_t$ laminate is more sensitive to initial longitudinal curvatures than a $[(\pm 45)_3]_t$ laminate. Interestingly enough, with no initial lateral curvature, neither laminate is sensitive to initial longitudinal curvatures. For the $[(\pm\theta)_3]_t$ family, in the presence of an initial lateral curvature, the cases of $\theta = 0°$, 15°, 30°, and 45° are less sensitive to the initial longitudinal imperfection than the other cases. The aluminum plate is more sensitive to longitudinal curvature than the $[(\pm 45)_3]_t$ case but it is not as sensitive as the $[(90_2/0_2/\pm 45)]_t$ laminate. With no initial lateral curvature, the aluminum plate is insensitive to longitudinal curvature.

EXPERIMENTAL SET-UP

Figure 7 shows how each plate was loaded in the experimental phase of the study. The purpose of the loading apparatus was to subject a portion of the plate to the conditions represented in the analysis. Each plate was 10 in. wide and over 20 in. long. Each end of a 20 in. lengthwise span of the plate was fastened to a steel shaft 12 in. long and 0.75 in. in diameter. The two shafts were parallel and a roller bearing was pressed onto each end of the two shafts. The bearings rolled freely on horizontally supported tracks. These tracks were in turn supported by a frame which held all components associated with the testing of the plates. Inside the 20 in. span two downward dead-weight loadings were applied. These

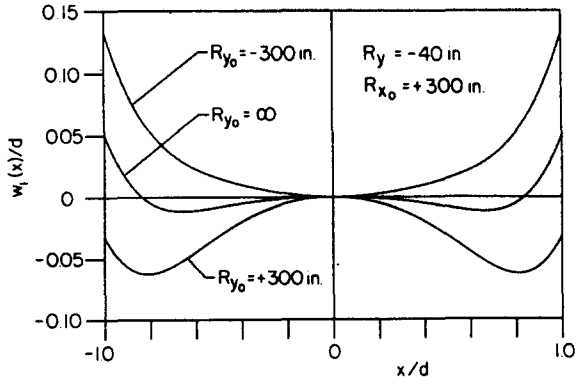

Fig. 5. Effects of initial longitudinal curvature on the deflections of a $[90_2/0_2/\pm 45]_t$ plate which has initial lateral curvature.

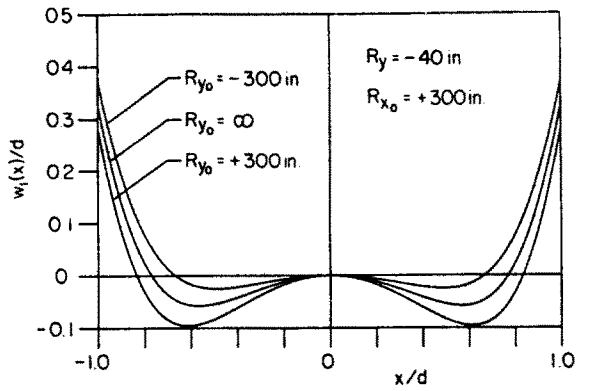

Fig. 6. Effects of initial longitudinal curvature on the deflections of a $[(\pm 45)_3]_s$ plate which has initial lateral curvature.

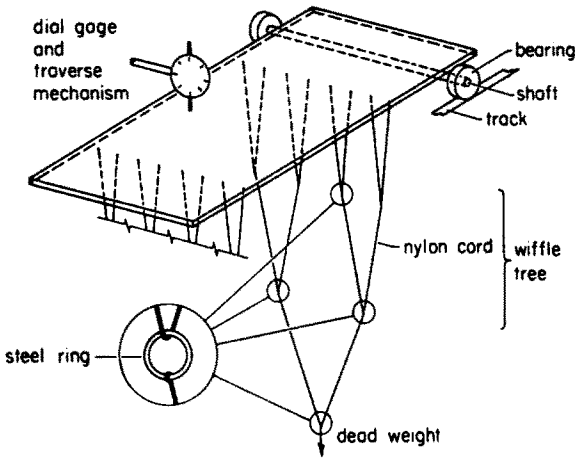

Fig. 7. Apparatus to load plates.

loadings were applied so as to simulate line loads across the width of the plate. The loads were equal in magnitude, 10 in. apart, and centered inside the 20 in. span. Each load was applied across the plate at eight discrete points by thin nylon chords. Steel rings and other pieces of nylon chord were used in a wiffle-tree arrangement to insure that only force conditions, as opposed to force and displacement conditions, were applied with the dead-weights. The region of the plate between the deadweight loads was then subjected to a pure bending moment and was considered the test region. Other loading arrangements could have been used but this one was easy to work with. One of the prime concerns was the effects of the plate being fastened to steel shafts. With this arrangement the out-of-plane displacement, slope, and curvature were constrained by the shaft. The slope and curvature were forced to zero while the displacement was constant along the shafts. There were no constraints where the dead weight loadings were applied. Would being fastened to shafts, as opposed to being supported by another system with no kinematic constraints, invalidate the assumption that the test region of the plate was being influenced only by pure bending moments? Analytical studies using linear plate theory indicated that neither the deflection response nor the fact that the midspan experienced pure moments seemed to be sensitive to distances between shaft supports or to distances between loadings for distances much shorter than were actually used. Other studies indicated that by far the most influential factor was the presence of any applied inplane load in the longitudinal direction. No such load was intentionally applied and the roller bearings prevented friction or other unwanted effects from restraining inplane motion. The dangers of using linear plate theory to size this experiment in nonlinear plate mechanics are well recognized. However, the whole purpose

of the experiment was to measure the out-of-plane deflections in a region where the plate was subjected to pure bending. Since the linear theory indicated the moment in the central portion of the plate was not influenced by boundary or load application conditions for spans which were quite short, in constructing the experiment these spans were liberally increased to account for uncertainties in the propagation of effects when the plate was responding nonlinearly. In addition, Bellow *et al.*[10] found that, at least for isotropic plates, their results were unaffected for span-to-width ratios as low as 1/3.

The out-of-plane deflections of the plate were measured with a dial gage. The gage was divided into 0.001″ increments and resolution in reading was taken to be one-half that amount. The dial gage was mounted on a mechanism which allowed it to traverse the full width of the plate. The mechanism could be used to precisely position the dial gage at a specific widthwise location on the plate. Thus the exact widthwise location at which the out-of-plane deflection was being measured was known to a high degree of accuracy. Both the initial, w_0, and final, w, out-of-plane displacements as a function of distance across the plate were measured with this device. The initial displacement measurements were used in a least-squares fashion to compute the initial lateral radius of curvature, R_{x_0}, which, recall, was assumed to be the same all across the plate width.

The displacements as a function of the longitudinal coordinate were also measured with the dial gage. It was clear after several measurements that the longitudinal radius of curvature of the loaded plates was indeed constant, as assumed, and precise point-by-point measurement of the loaded longitudinal radius of curvature was not necessary. A straightedge was subsequently used to measure the longitudinal dip in the plate, the length of the straightedge and the magnitude of the dip being used to compute R_y. The dial gage technique and least-squares data reduction were still used, however, to compute the initial longitudinal radius of curvature, R_{y_0}.

The composite plates used in the study were fabricated from T300/5208 prepreg tapes 6 in. wide. Both composite plates averaged 0.062 in. in thickness. The plates were fabricated to be flat but indeed did have small but noticeable initial curvatures. The numerical studies of the plates indicated that the sign of the initial curvatures could be important. Thus the sides of the plate were identified as side 1 and side 2, the idea being that the plate could be tested with one side up, to have one initial curvature, and then tested again, with the other side up, to have the opposite initial curvature. This, as will be discussed, did not work out exactly as hoped.

COMPARISONS BETWEEN EXPERIMENT AND THEORY

Figure 8 shows the initial lateral shape of the $[(\pm 45)_3]_s$ plate as measured with the dial gage at midspan. In the figure, the side of the plate designated as side 1 is up. Henceforth all results for all plates will be for the side 1 up configuration. Plotted are the out-of-plane deflections as a function of the lateral coordinate. The deflection of the center of the plate was arbitrarily set to zero. In reality, the least-squares fit to the data was set to zero at the center. A least-squares analysis of the data produced an initial lateral radius, R_{x_0}, of

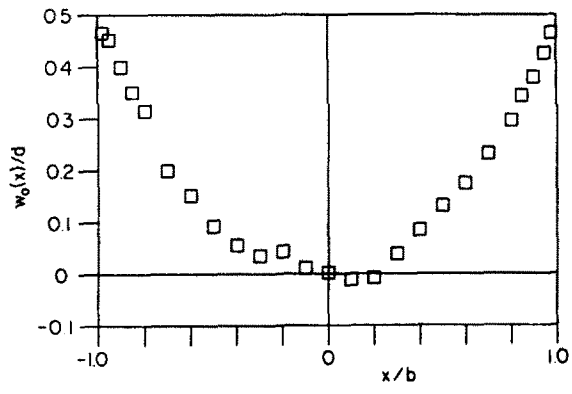

Fig. 8. Initial lateral shape of $[(\pm 45)_3]_s$ plate.

curvature of 409 in. The no-load longitudinal deflection data looked similar to Fig. 8. The value of R_{y_0} was found to be -299 in. Figure 9 shows the theoretically predicted and experimentally measured deflections of the plate due to a range of bending moments. Figure 9(a) shows the results for what can be considered a small bending moment, 4.8 in-lb. This level of moment produced a radius of curvature of -160 in. in the longitudinal direction. With this level of load, the plate response was linear. Figures 9(b) and 9(c) illustrate the plate response for higher levels of moments. With 10 in-lb. of load, Fig. 9(b), flattening of the plate was beginning. With 25.3 in-lb., strictly nonlinear behavior was predicted and was exhibited. In examining these and to-be-discussed figures, it is important to indicate how the theoretically predicted results were generated. As was previously stated, R_y was considered a

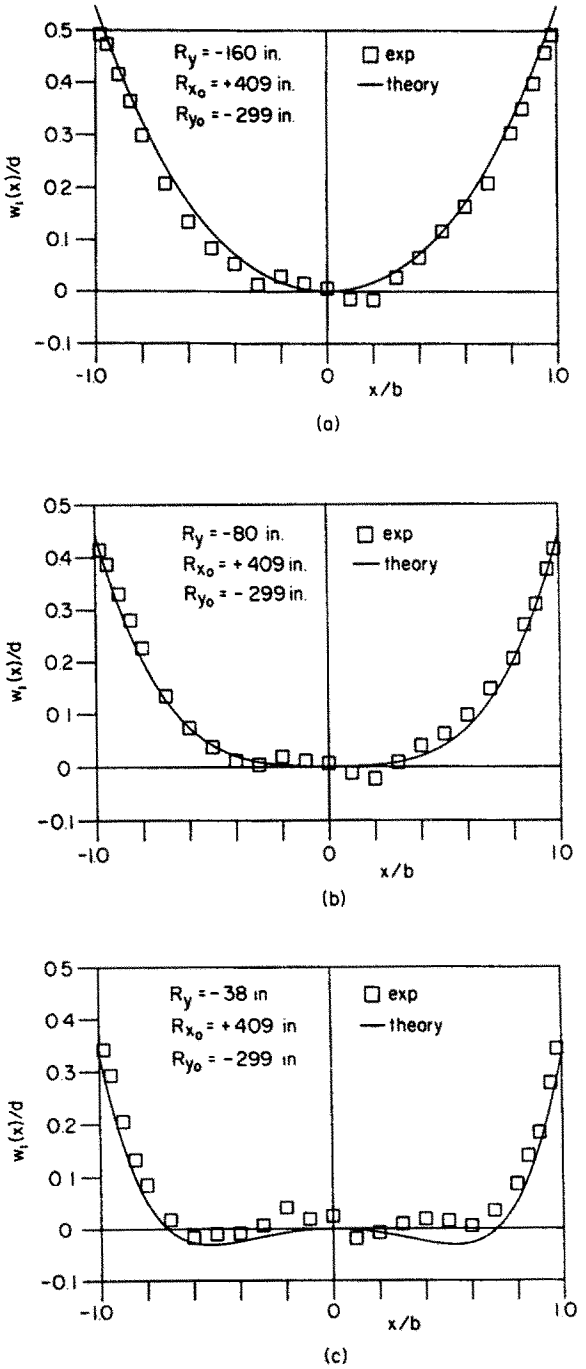

Fig. 9. Comparison of deflections for $[(\pm 45)_3]_s$ plate with increasing levels of applied moment: (a) 4.8 in.-lb.; (b) 10 in.-lb.; (c) 25.3 in.-lb.

known independent parameter in the problem. Thus, R_y was measured experimentally at each load level. This value of R_y, along with the experimentally determined values of R_{x_0} and R_{y_0}, were then used in the analysis to predict the out-of-plane deflection response. It was this response that is being compared to the experimental measurements. Equation (31) was used to determine, theoretically, what level of applied moment was required to produce the particular value of R_y. This theoretically calculated value of moment could be compared with that actually applied by the deadweight loading. Table 1 compares moments for each of the experimental load levels used for the $[(\pm 45)_3]_s$ plate.

Figure 10 shows the initial shape of the $[(90_2/0_2/\pm 45)]_s$ plate. Figures 11(a–d) show the cross-sectional shape for four moment levels. The initial lateral curvature of this plate was found to be +403 in. while the initial longitudinal curvature was −2051 in. This value of initial longitudinal curvature has such a small effect on plate response the plate could have been considered flat in the longitudinal direction. From the figures, it is clear that the trends are correctly predicted but the correlation is not as good as for the $[(\pm 45)_3]_s$ plate. Recall, though, that the parameter studies of the NUMERICAL RESULTS section showed the $[(\pm 45)_3]_s$ plate to be much less sensitive to the various parameters of the problem than the $[(90_2/0_2/\pm 45)]_s$ plate was. Thus better correlation could have been expected for the $[(\pm 45)_3]_s$ plate. Table 2 lists the moment comparisons for the $[(90_2/0_2/\pm 45)]_s$ plate.

Figure 12 shows the initial shape for the aluminum plate. The initial lateral curvature was measured to be 197 in. while the initial longitudinal curvature was measured to be −1027 in. Figures 13(a–d) show the shape of the plate for four increasing load levels. The correlation between theory and experiment for the aluminum is comparable to the correlation for the $[(\pm 45)_3]_s$ case and can be considered quite good. Table 3 shows a comparison of measured and computed moments for the four load levels applied to the aluminum plate.

Table 1. Data for $[(\pm 45)_3]_s$ plate, $R_{x_0} = 409$ in., $R_{y_0} = -299$ in.

Experimentally Applied Moment (in.-lb.)	Experimentally Measured R_y (in.)	Calculated Applied Moment eq. 31 (in.-lb.)
4.8	-160	6.1
10.0	-80	12.9
25.3	-38	25.3

Table 2. Data for $[90_2/0_2/\pm 45]_s$ plates, $R_{x_0} = +403$ in., $R_{y_0} = -2051$ in.

Experimentally Applied Moment (in.-lb.)	Experimentally Measured R_y (in.)	Calculated Applied Moment eq. 30 (in.-lb.)
7.5	-288	8.6
13.7	-165	15.3
25.3	-105	24.3
65.3	- 40	65.4

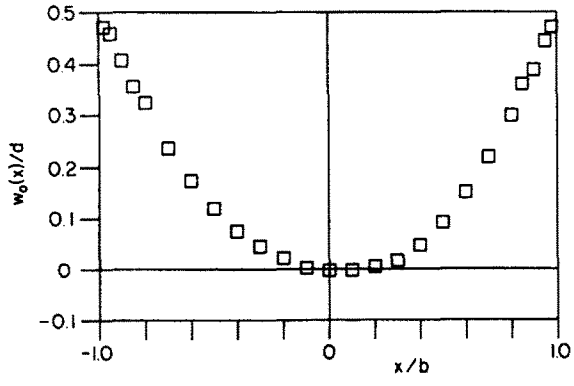

Fig. 10. Initial lateral shape of $[90_2/0_2/\pm 45]_s$ plate.

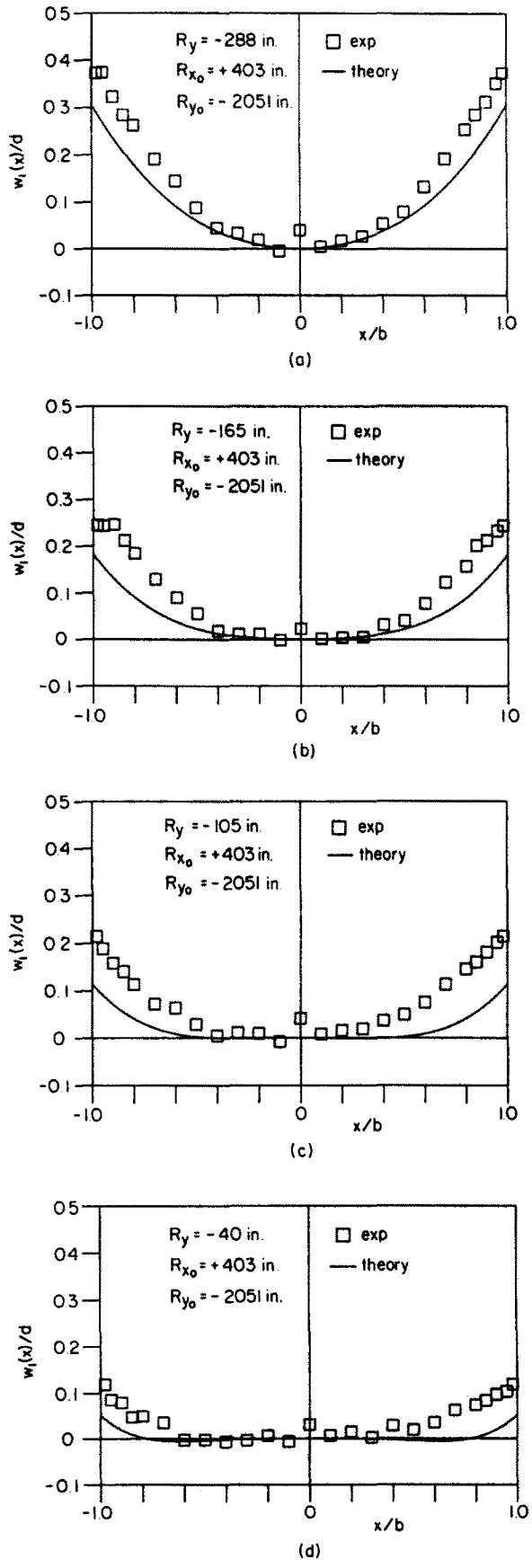

Fig. 11. Comparison of deflections for $[90_2/0_2/\pm 45]$, plate with increasing levels of applied moment: (a) 7.5 in.-lb.; (b) 13.7 in.-lb.; (c) 25.3 in.-lb.; (d) 65.3 in.-lb.

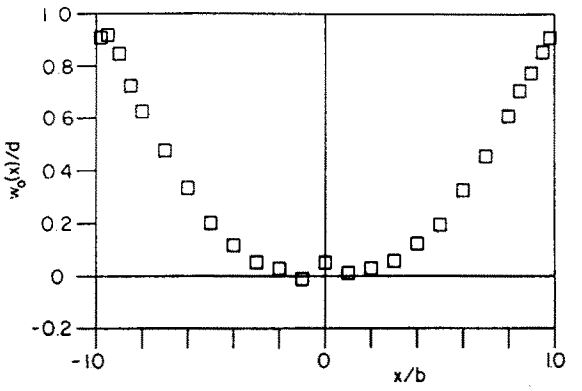

Fig. 12. Initial lateral shape of aluminum plate.

Table 3. Data for aluminum plate, $R_{x_0} = 197$ in., $R_{y_0} = -1027$ in.

Experimentally Applied Moment (in.-lb.)	Experimentally Measured R_y (in.)	Calculated Applied Moment eq. 30 (in.-lb.)
4.8	-384	12.4
10.0	-210	16.7
25.3	-90	27.7
50.3	-45	50.8

DISCUSSION

From the experimental results, it is evident that for all plates tested, the anticlastic curvature was suppressed when the bending moments became large. The plates were deformed more into a cylindrical shape than into a saddle shape. For example, for the $[(90_2/0_2/\pm 45)]_s$ plate with 65.3 in-lb of moment, Fig. 9(d), the peak-to-peak deflections across the width of the plate were less than one-tenth the plate thickness. Yet in the longitudinal direction, due to R_y, the dip along the 10 in. span between deadweight loads was over 5 plate thicknesses. Also from the results, it is clear the theory can predict the phenomenon quite accurately. This is true for the composite plates as well as the aluminum plate. The theory works for what could be considered a soft-in-bending composite plate, the $[(\pm 45)_3]_s$, as well as a stiffer composite plate, the $[(90_2/0_2/\pm 45)]_s$. Apparently using average values of R_{x_0} and R_{y_0} and assuming there is no initial twist curvature is not a bad first approximation. However, the issue of twist curvature needs further discussion. In the experimental set-up, the two steel shafts, to which the plates were attached, were parallel to each other. Thus overall, there was no twist curvature in the unloaded plates. On-the-whole, the assumption of no twist curvature was an actual representation of the experiment. However, there was another issue involved with the shape of the unloaded plates. The issue is complex and almost beyond the scope of the paper. However, it affected the experiments here and will be discussed briefly. The issue is as follows: The various problems associated with not being able to obtain a perfectly flat laminate also lead to elastic properties which are not symmetric with respect to the laminate's geometric mid-plane. A misaligned ply, for example, leads to small values of the B_{ij} matrix. Lack of uniform curing through the thickness leads to the same lack of symmetric elastic properties. These unsymmetric elastic properties couple with another inherent aspect of composite fabrication, namely residual inplane stress. Because of the elevated temperature cure of the epoxies, there are residual stresses in the laminate at room temperature. These residual stresses, coupled with asymmetry of the elastic properties through the thickness, can be visualized as inplane loads acting slightly off the midplane, i.e. an eccentric loading. If the magnitude of the various effects is just right this can lead to what can be considered as a generalization of the oil canning phenomenon, i.e. the laminate would snap from one equilibrium configuration to another. An extreme and often observed case of this is described in detail by Hyer[12–14].

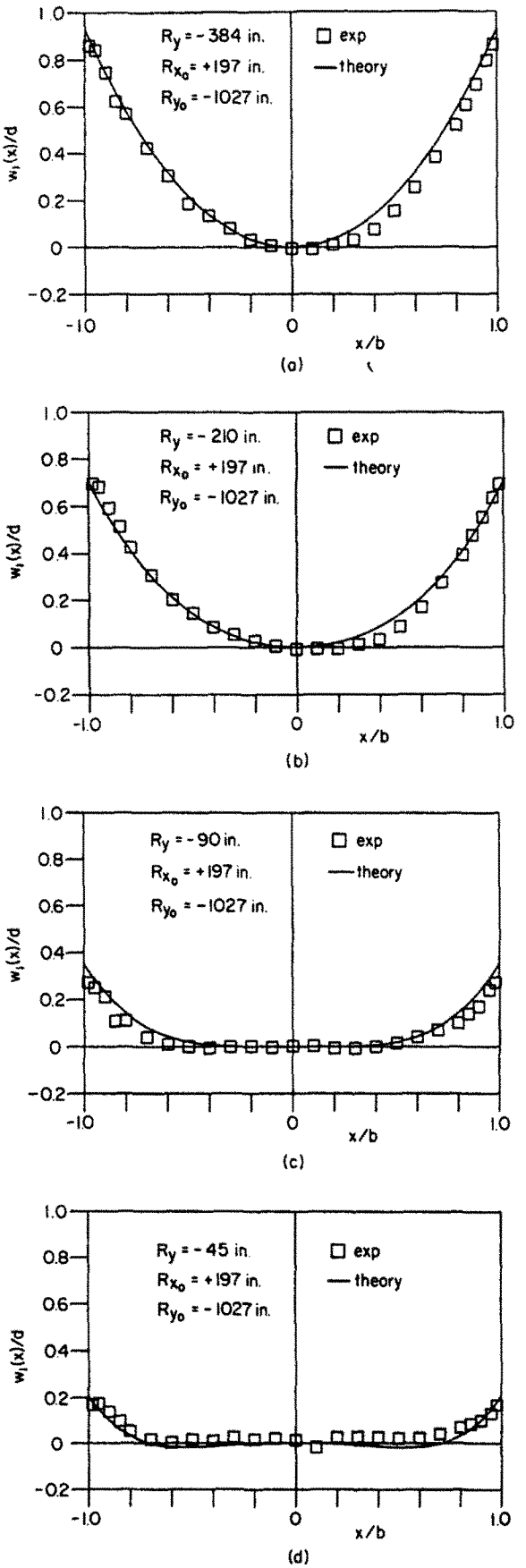

Fig. 13. Comparison of deflections for aluminum plate with increasing levels of applied moment: (a) 4.8 in.-lb.; (b) 10 in.-lb.; (c) 25.3 in.-lb.; (d) 50.3 in.-lb.

In the laminates here, the effect was not extreme but it was there. The slight initial curvature of each composite plate was due in part to such effects. The curvature of a particular plate was not necessarily unique and a very soft snap-through, requiring practically no force, could be detected. Thus, if the plate was tested with side 2 up, the initial curvatures were not of opposite sign to the curvatures of the side 1 up configuration. The attaching to the parallel shafts and artificially eliminating the overall twist curvature, the change in direction of the plate's own dead weight, and the tendency to snap softly, all combined to prevent the side 2 up initial curvatures from being a simple sign-switch of the side 1 up configuration. For the aluminum plate, however, there was the simple sign switch. The initial shape at the aluminum plate was more than likely due to plastic bending deformations as opposed to eccentric residual inplane loads and elastic deformations. These plastic deformations could well have resulted from the rolling of the 0.0625" plate or from shipping or storage. However, when the initial deformations of the various plates in the side 2 up configuration were measured and the plates loaded, the correlation between the theory presented here and experiment was good.

The poor correlation between the calculated moments and the applied moments, Tables 1–3, for the low load levels is also felt to be due to the form of the initial imperfections. Inspection of the initial out-of-plane deflection data indicated that although a constant value of R_{x_0} was a reasonable first approximation, the initial shapes were not, for example, symmetrically disposed about $x = 0$, as eqn (18) assumed. For a small load, this is important. If for the moment the plate is likened to a wide beam, the initial R_{x_0} curvature contributes to the moment of inertia, I. Slight changes in R_{x_0} lead to changes in I which ultimately affect the response of the wide beam. At low load levels, the exact initial value of R_{x_0}, and how it varies across the width, seriously affects the wide beam response. However as the load is increased and, due to nonlinear effects, the plate flattens laterally, the overall value of R_{x_0}, as opposed to the exact details, governs the response. Thus at the low load level, moment-curvature response from the theory would not correlate as well with the experiment as it would at the high load levels.

REFERENCES

1. G. F. C. Searle, *Experimental Elasticity, A Manual for the Laboratory*, pp. 38–58. University Press, Cambridge (1908).
2. H. Lamb, On the flexure of a flat elastic spring. *Phil. Mag.* 182–188 (1891).
3. D. G. Ashwell, The anticlastic curvature of rectangular beams and plates. *J. Royal Aeronaut. Soc.* **54**, 708–715 (1950).
4. D. G. Ashwell and E. D. Greenwood, The pure bending of rectangular plates. *Engineering*, 21 July, p. 51 and 28 July, p. 76 (1950).
5. D. G. Ashwell, A characteristic type instability in the large deflexions of elastic plates—I. Curved rectangular plates bent about one axis—II. Flat square plates bent about all edges. *Proc. Royal Soc.* **A214**, 98–118 (1952).
6. G. Gerard, Note on beams and plates. *J. Aeronaut. Sci.* **19**, 207–208 (1952).
7. Y. C. Fung and W. H. Wittrick, The anticlastic curvature of a strip with lateral thickness variation. *J. Appl. Mech.* **21**, 351–358 (1954).
8. Y. C. Fung and W. H. Wittrick, A boundary layer phenomenon in the large deflexion of thin plates. *Quart. J. Mech. and Appl. Math.* **VIII**, Part 2, 191–210 (1955).
9. R. J. Pomeroy, The effect of anticlastic bending on the curvature of beams. *Int. J. Solids Structures* **6**, 277–285 (1970).
10. D. G. Bellow, G. Ford and J. S. Kennedy, Anticlastic behavior of flat plates. *Experimental Mech.* **5**(7), 227–232 (1965).
11. Y. C. Pao, Simple bending analysis of laminated plates by large-deflection theory. *J. Composite Materials* **4**, 380–389 (1970).
12. M. W. Hyer, Some observations on the cured shapes of thin unsymmetric laminates. *J. Composite Materials* **15**, 175–194 (1981).
13. M. W. Hyer, Calculations of the room-temperature shapes of unsymmetric laminates. *J. Composite Materials* **15**, 296–310 (1981).
14. M. W. Hyer, The room-temperature shapes of four-layer unsymmetric cross-ply laminates. *J. Composite Materials* **16**, 318–340 (1982).
15. J. E. Ashton and T. S. Love, Experimental Study of the stability of composite plates. *J. Composite Materials* **3**, 230–242 (1969).
16. R. M. Jones, *Mechanics of Composite Materials*. McGraw-Hill, New York (1974).